SI Appendix

Preservation/Identification of Flood-Deposited Sediment on Stalagmite Surfaces. In addition to those discussed in the text, several factors influence our ability to link TCs to cave flooding:

Distance vs Intensity Relationships - Large storms distal to the cave may produce rainfall events commensurate with more proximal but smaller storms. Studies of South Pacific TCs found a pronounced decrease in rainfall with distance, particularly after 600-700 km from the eye of the storm (1). Thus, in order to test the 600 km radius window we used to develop our calibration, we also calculated the peak annual single and multi-day rainfall totals for TCs within 500 km (Fig. S7). The differences in results between the 500- and 600-km buffers are minor, with most of the offset for low rainfall values; all the large events are still associated with TCs.

Closely Occurring TCs - TCs routinely occur in close succession within a single season. For example, TC Fay and TC Evan both passed within 400 km of KNI-51 during March 2004, and TC Debbie reached a similar distance in December 2003. Because flooding of the cave is required to deposit mud on stalagmite caps, and because stalagmite growth may not occur immediately after floodwaters recede, multiple TCs within the same season may not be individually recorded or be distinguishable from one another.

TC Track and Speed – Rainfall intensity at a site is a function of the residence time of a storm and the path the storm has followed to that site. TCs weaken rapidly over land and thus wind speeds and rainfall amounts typically decrease markedly after landfall (2). However, circular storm tracks may increase the time a storm impacts a given site and thereby increases rainfall totals there. For example, in February 2011, TC Carlos made landfall near Darwin and doubled back on the area, dropping 684 mm of rain in the process. However, its subsequent track took it inland to the west where rainfall of only 90 mm was recorded at Wyndham several days

later. In 1986, within error of the largest mud layer in KNI-51-11, TC Hector made landfall just northeast of KNI-51, resulting in intense rainfall that caused 200-year flooding on the Fitzroy River and the evacuation of hundreds of people from nearby Wyndham. Rainfall associated with this event reached the 90th percentile for all Januaries on record (from 1898) at Carlton Hill Station. In addition, TC Carlos tracked close to KNI-51 in February 2011, dropping 90 mm of rain; TC Lua made landfall in western Kimberley in 2012, with three-day rainfall of >500 mm.

Storage Effects – Cave flooding should reflect not only the rainfall associated with a particular storm event but also the available water storage space in the watershed and in the bedrock overlying the cave. Thus, long-term area and cave-specific monitoring is required to formally define the exact nature of the cave flood threshold. However, drips had ceased in KNI-51 when visited in June 2009 and June 2011, approximately 1-2 months after the end of the monsoon season, suggesting limited storage capacity above this cave.

Changes in Growth Direction – The thickest mud layers in stalagmite KNI-51-11 are associated with a change in growth direction, suggesting that the stalagmite shifted its position on its mud substrate during large flood events. Such a change in geometry complicates age-distance relationships between radiometric dates and can interfere with the preservation of mud on the stalagmite cap. This problem is limited here due to the high density of high-precision dates. Growth direction changed several times during its history, each time in association with a thick layer of sediment (Type 3 layer).

Diagenetic Alteration – Isolated areas in sample KNI-51-O are recrystallized from finely crystalline primary aragonite to more coarsely crystalline calcite. Where such alteration has occurred, the change in crystal fabric obscures mud layers, making their identification/ classification slightly more difficult. In this case, however, affected portions are on a cm-scale

near the central growth axis and in no cases were entire growth bands fully obscured. Thus, mud layers were easily discernable, and these areas were avoided for dating. Relatedly, no dissolution or alteration is apparent on any growth surfaces (bounding layers) immediately below mud layers as would have occurred if dripwater had become corrosive prior to cave flooding (3).

Modern environmental setting. Onset of IASM rainfall in the Kimberley typically occurs in mid- to late December, with the poleward displacement of the subtropical jet and ridge. Tropical cyclone genesis regularly occurs in association with the monsoon trough which separates trade wind easterlies on its southern side from westerly winds between the monsoon trough and the equator, and slopes towards the equator with increasing height (4). The position of the monsoon shear line over northwestern Australia relates to the Pilbara Heat Low, reflecting landmass diabatic forcing and limiting the poleward extent of the summer monsoon regime. The monsoon trough extends well north of the continent with maximum cloudiness located at 0 to 5ºS and 5˚ to 10ºS. Over the region of the Maritime Continent the high SSTs provide a broad, ill-defined area of strong convection, indicated by the outgoing longwave radiation (OLR) pattern over the region, which can be strikingly different from the well-defined structure and latitudinal position of the OLR patterns associated with the intertropical convergence zone over the adjacent Pacific and Indian oceans (5). The onset corresponds to a dramatic increase in zonal winds over an approximately 90˚ longitude region. The strong convection that is contained within the westerly flow, extends over a large region, and locates monsoon depressions.

Possible effects of humans on surface hydrology and the KNI-51 flood record. There can be no doubt that the ecosystems of the Australian tropics have been strongly influenced by human

activity, starting with burning by Aboriginal peoples in the late Pleistocene (6) and including pastoral and agricultural practices by descendants of European settlers beginning in the 19th century. Cattle grazing in the eastern Kimberley, including at Carlton Hill Station, began in the late 19th century (7). The denudation of some plant species, coupled with soil compaction and other effects associated with the introduction of cattle has been shown to increase run-off and soil erosion rates (8-9), and thus we interpret the large spike in cave flooding events in the 1890s likely as reflective of changes in land-use practices. If so, then the sensitivity of cave flooding to rainfall during the calibration period (1906-1986 CE) may have been somewhat greater relative to the earlier portions of the stalagmite record. However, it is unclear what impact these changes had on our rainfall/flood event calibration, and this does not change the underlying facts that TCs contribute the majority of extreme rainfall events and that the highest rainfall totals are logically the most likely to be associated with flooding. Similarly, it is worthwhile considering the susceptibility of the full range of our flood layer time series (the last 2200 years) to prehistoric landscape changes, but little independent evidence exists for substantive human-induced changes to vegetation type over this time (10-12).

References

1 - Villarini, G. *et al*. (2014) Sensitivity of tropical cyclone rainfall to idealized global scale forcings. *J Clim* 27: 4622-4641.

2 - Vickery P, Masters F, Powell M, Wadhera D (2009) Hurricane hazard modeling: The past, present, and future. *Jour Wind Eng Ind Aero* 97: 392 – 405.

3 – Railsback L, Akers P, Wang L, Holdridge G, Voarintsoa N (2013) Layer-bounding surfaces in stalagmites as keys to better paleoclimatological histories and chronologies. Int J Speleo

42: 167–180.

4 - McBride J (1987) The Australian summer monsoon. In: C. P. Chang and T. N. Krishnamurti (eds), Monsoon Meteorology. Oxford University Press, New York, 203–231.

5 - Walliser D, Gautier C (1993) A satellite-derived climatology of the ITCZ. *J Clim* 6: 2162-2174.

6 - Miller G, Magee J, Fogel M, and Gagan M (2007) Detecting human impact on the flora, fauna and summer monsoon of Pleistocene Australia. *Clim Past* 3: 463–473.

7 - Durack (1972) Australian Dictionary of Biography; http://adb.anu.edu.au/biography/durack-patrick-3457.

8 - Bartley, R. *et al*. (2006) Runoff and erosion from Australia's tropical semi-arid rangelands: influence of ground cover for differing spaces and time scales. *Hydrol Proc* 20: 3317-3333.

9 - Carroll, C. *et al*. Sediment erosion research in the Fitzroy basin central Queensland: an overview. 19th World Congress of Soil Science, Soil Solutions for a Changing World 167 1 – 6 August 2010, Brisbane, Australia (2010).

10 - McGowan H, Marx S, Moss P, Hammond A (2012) Evidence of ENSO mega-drought triggered collapse of prehistory Aboriginal society in northwest Australia. *Geophys Res Lett* 39: L22702.

11 - van der Kaars S, De Deckker P, Gingel F (2006) A 100 000-year record of annual and seasonal rainfall and temperature for northwestern Australia based on a pollen record obtained offshore. *J Quat Sci* 21: 879-889.

12 - Denniston R *et al*. (2013) A Stalagmite Record of Holocene Indonesian-Australian Summer Monsoon Variability from the Australian Tropics. *Quat Sci Rev* 78: 155-168; 10.1016/j.quascirev.2013.08.004.

Fig. S1. KNI-51 stalagmites discussed in this study. For ease of presentation, scales of individual samples were adjusted individually but cm demarcations are visible along central growth axes.

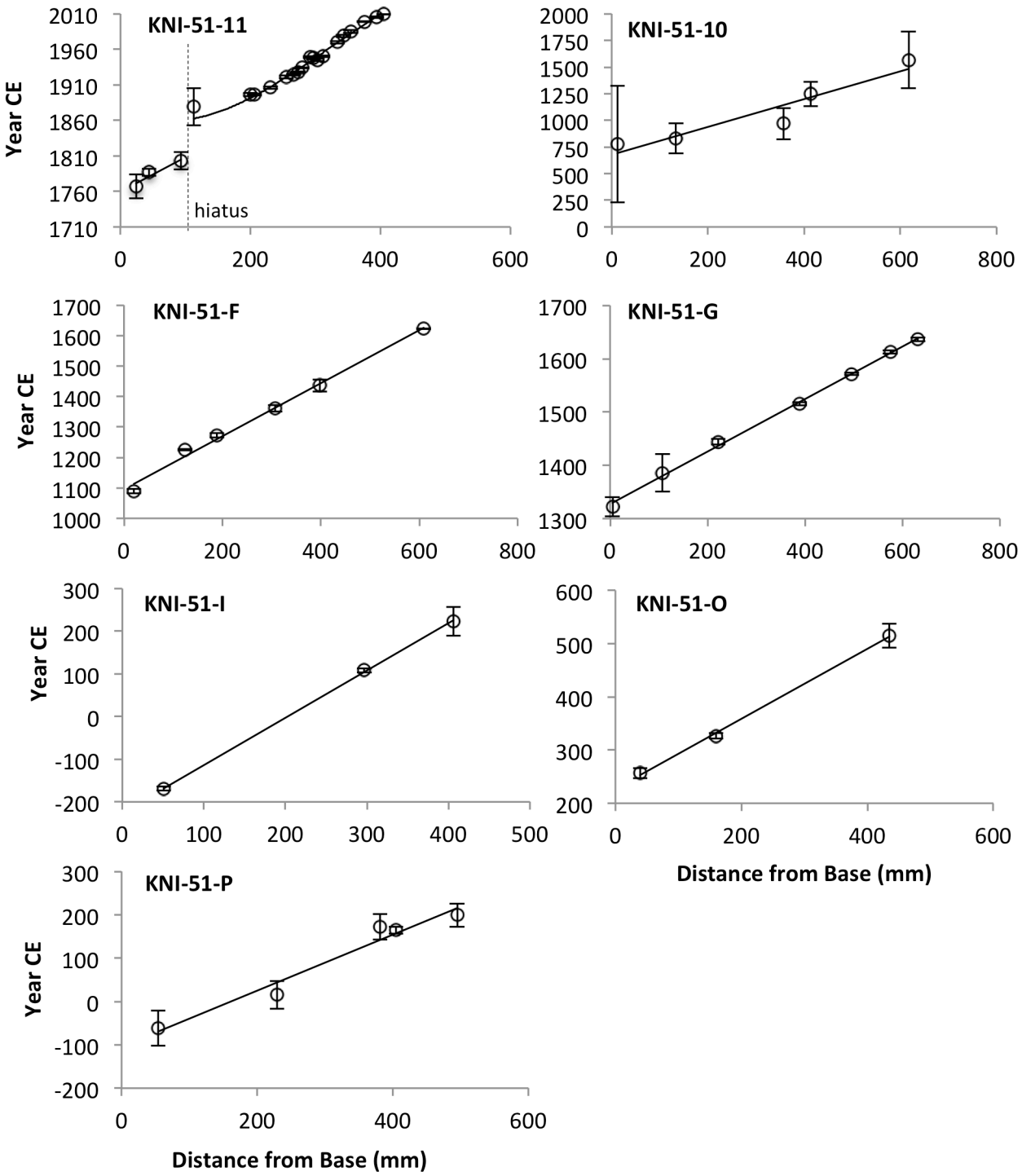

Fig. S2. ^{230}Th dates and age models. Vertical lines represent 2 standard deviation errors. Dates for all stalagmites other than KNI-51-11 are from ref. 11.

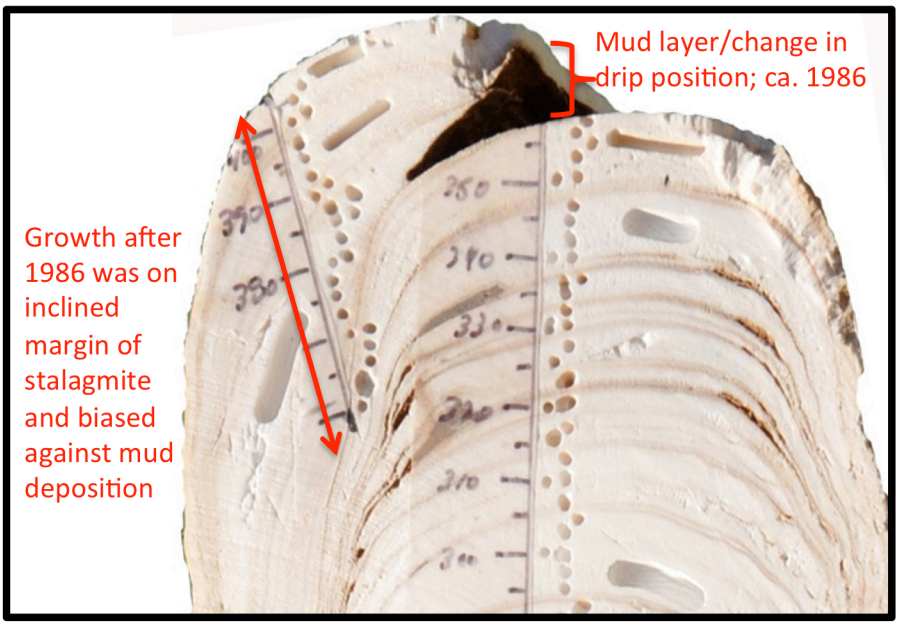

Fig. S3. Top of stalagmite KNI-51-11 showing change in growth position after ~1986 CE that resulted in an inclined margin that appears to have limited preservation of flood-derived sediment. Given its geometry, it is likely that following retreat of cave floodwaters, re-establishment of drips onto the active growth surface were highly effective at eroding any flood-derived sediment. A more horizontal growth surface did not re-develop until approximately 2008.

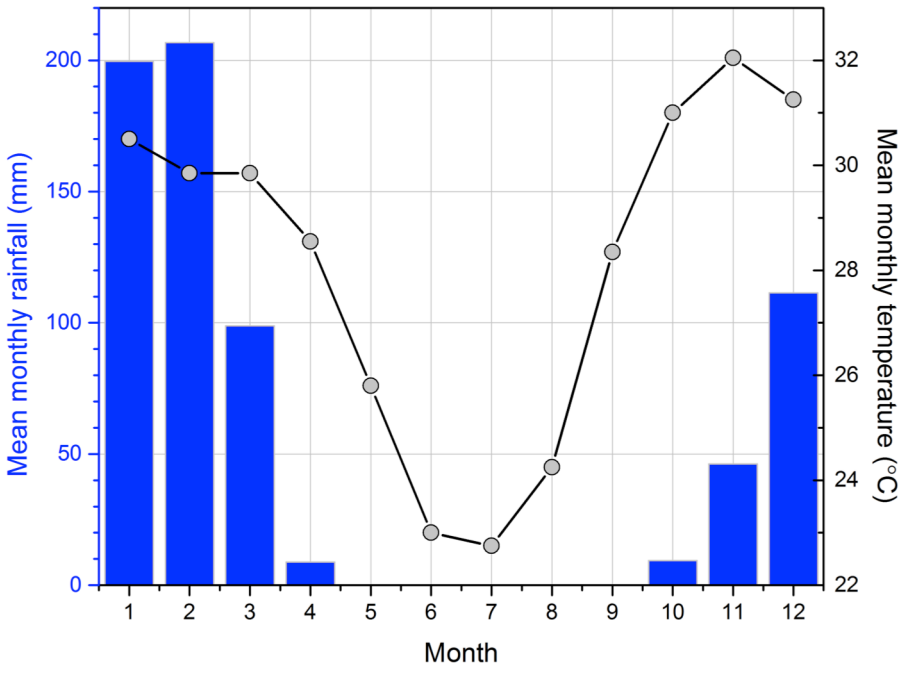

Fig. S4. Monthly rainfall (blue bars) and temperature (grey circles) values from the town of Kununurra, Western Australia, located approximately 50 km from KNI-51 (www.bom.gov.au).

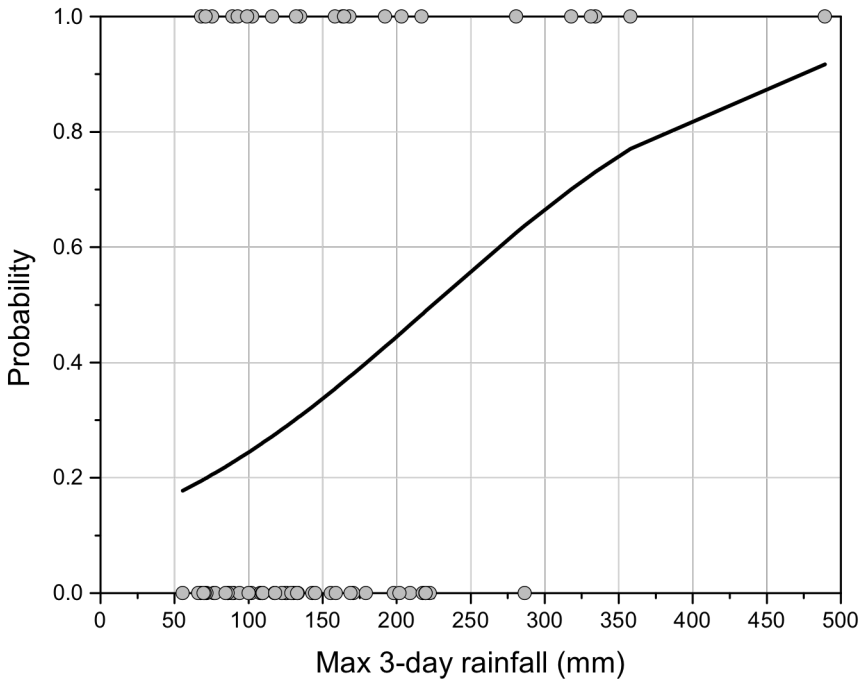

Fig. S5. Logistic model of rainfall thresholds for cave flooding events. The values "1" and "0" represent the occurrence and non-occurrence of a flood event, respectively, for different values of maximum three-day rainfall. The black line represents the fitted logistic model; p-value<0.015.

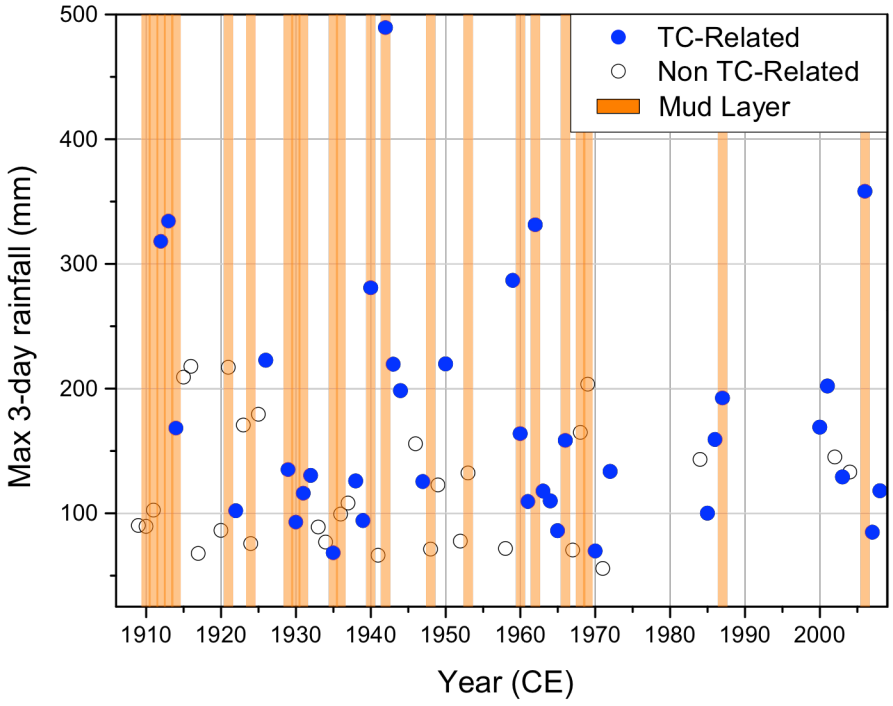

Fig. S6. Three-day peak annual rainfall totals (blue circles for events tied to TCs and white circles for events tied to non-TC rainfall) for Carlton Hill Station with correlations to flood layers (vertical orange bars) from stalagmite KNI-51-11. Ages of the flood layers have been shifted by up to ±1 yr (minimum age uncertainties from ^{230}Th dates) to determine a maximized correlation with three-day peak rainfall events. In doing so, the ages of all mud layers were shifted uniformly, the most conservative possible tuning method, rather than individually which would have yielded a higher correlation. Gaps in the record represent periods of incomplete rainfall data collection. In most cases, the highest rainfall totals are associated with TCs and can be temporally aligned with stalagmite flood events.

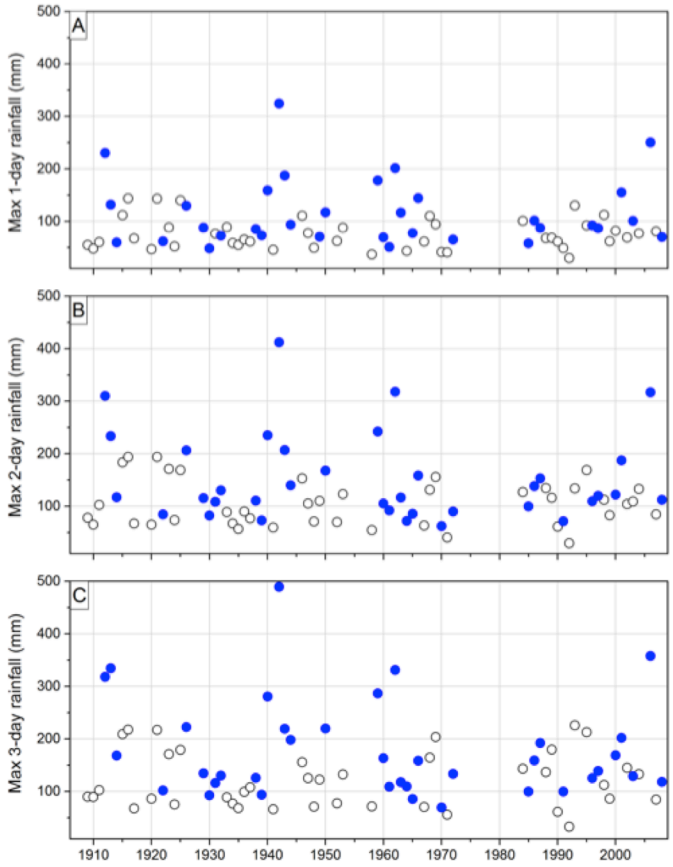

Fig. S7. From A-C: Peak annual consecutive 1-, 2-, and 3- day rainfall totals for Carlton Hill Station for the period of calibration (x-axis in years CE) using a 500 km radius window. Gaps represent periods of incomplete data collection at the station. Blue circles denote rainfall derived from TCs within 500 km radius of KNI-51, while open circles denote rainfall associated with events not assigned to TCs.

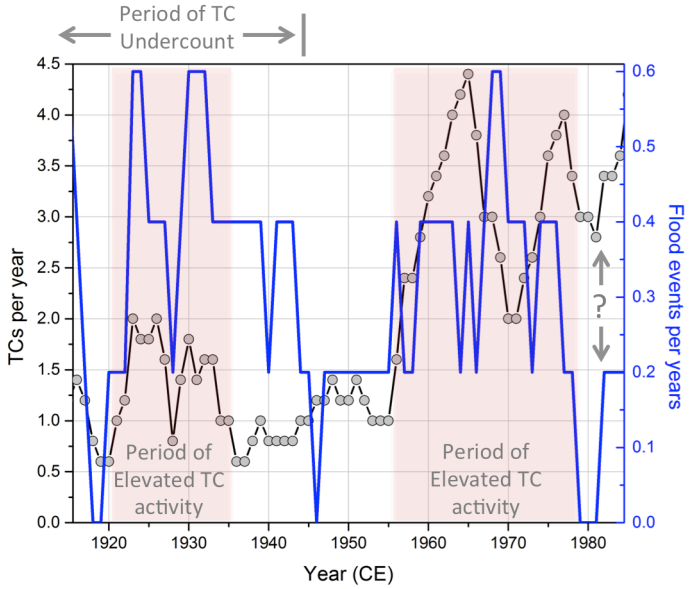

Fig. S8. Five-year running means of observed TC events within 600 km of cave KNI-51 for the period 1908-1986 CE (black line) with flood events from stalagmite KNI-51-11 (blue line). The accuracy of the TC count likely declines prior to the start of the satellite era (1970 CE) and this undercount is particularly evident in the interval of peak TC activity from 1920-1935. Increases in TC activity are recorded for the same intervals (pink shaded areas) in both the historical and stalagmite records. TC track data were obtained from www.ncdc.noaa.gov/ibtracs/index.php?name=ibtracs-data.

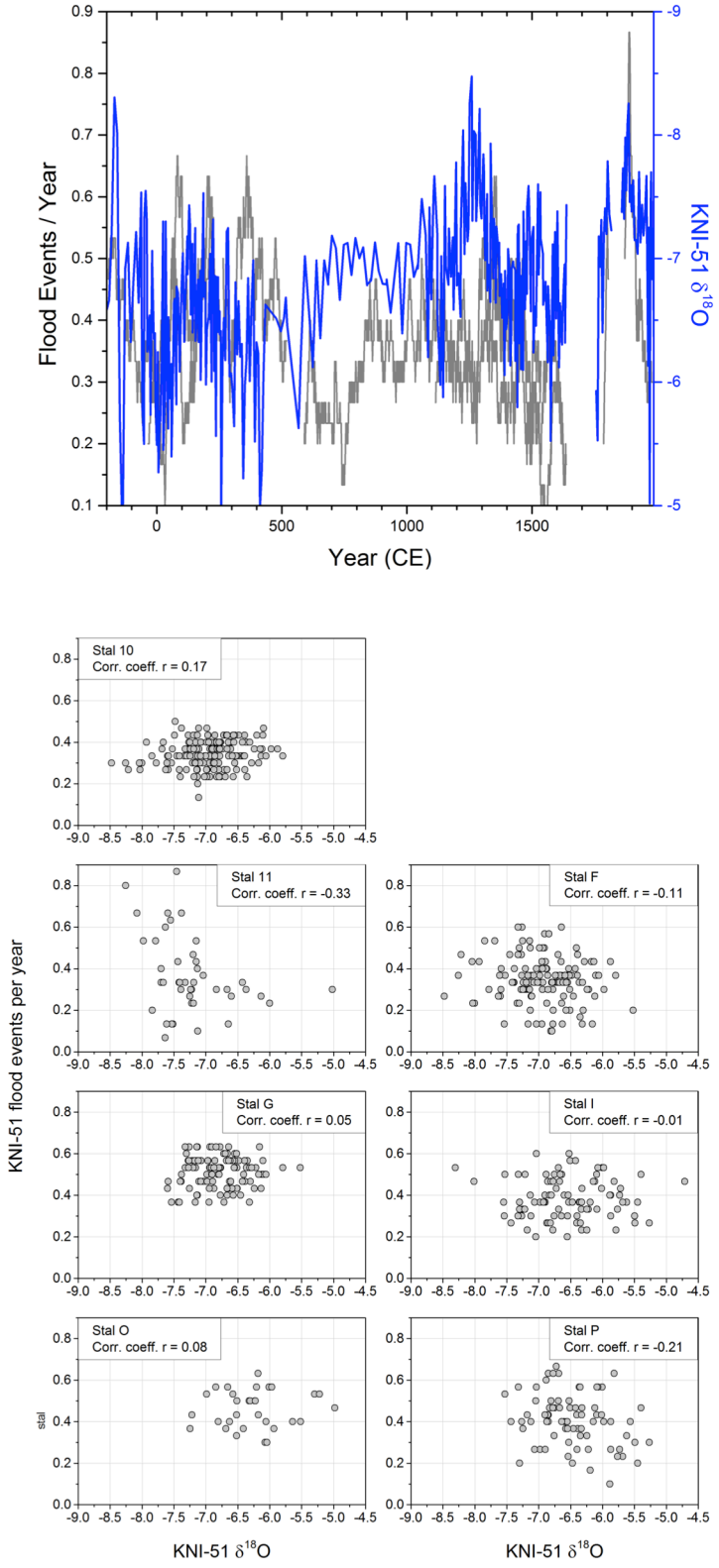

Fig. S9. Top: Flood layer and IASM variability. Comparison of KNI-51 flood record (grey line) with IASM reconstruction derived from oxygen isotopic values from the same stalagmites[8] (blue). Flood layer values from KNI-51-G were reduced by 0.2 to account for observed offset. Stronger IASM is up on the y-axis. Bottom: Correlation between oxygen isotopic ratios and flood events from individual KNI-51 stalagmites. A negative correlation would result from a strengthened monsoon which would increase the likelihood of cave flooding while simultaneously enhancing amount effect-related ^{18}O depletion in rainwater.

Fig. S10. Mud layer types (T). Majority of the sediment associated with the Type 3 layer (right panel) has been removed. Linear trough is area milled for dating. Note that stalagmite growth surfaces associated with mud layers do not appear to suffer from corrosion, suggesting rapid submersion by floodwaters. Mud preservation is typically most evident on the margins of stalagmite growth surfaces, likely because dripwaters erode newly deposited mud from central growth axis.

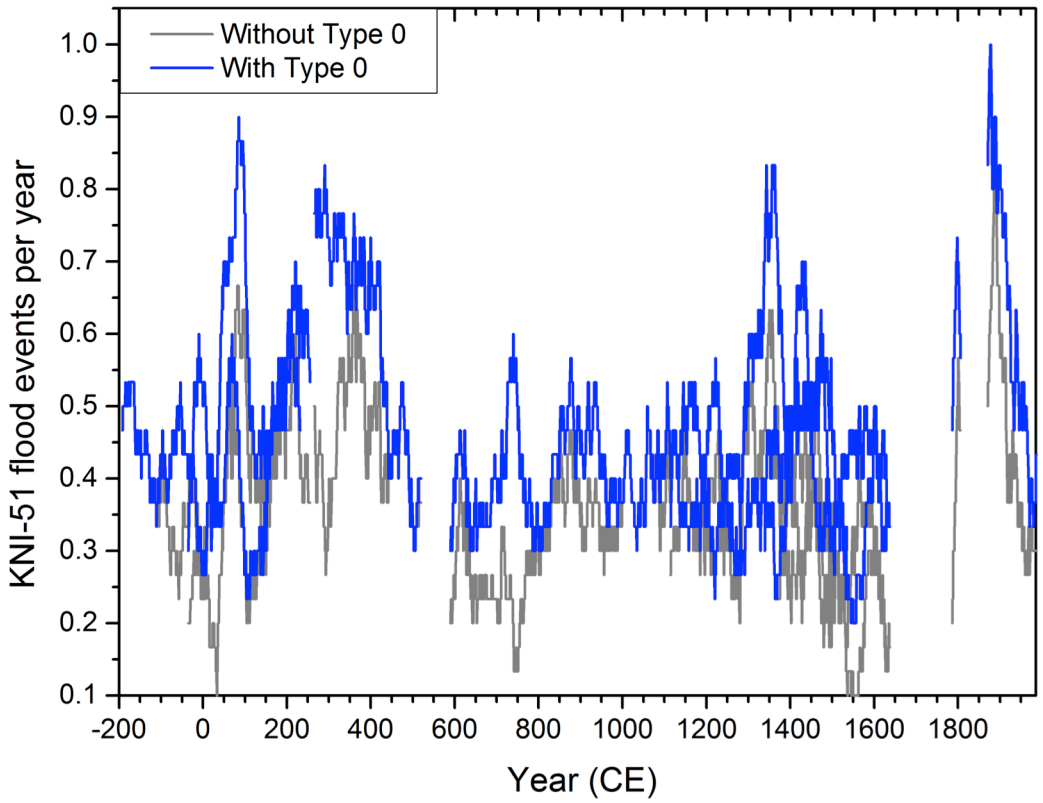

Fig. S11. Influence of Type 0 mud layers on flood layer time series. Composite flood layer time series including (grey line) and excluding (blue line) Type 0 mud layers. Type 0 flood layers were excluded from the primary flood reconstruction because their nature and origin is unclear, but may be an artifact of biases in mud layer preservation. This figure provides a qualitative test of the impact of including these layers and reveals a minimal impact on temporal trends.

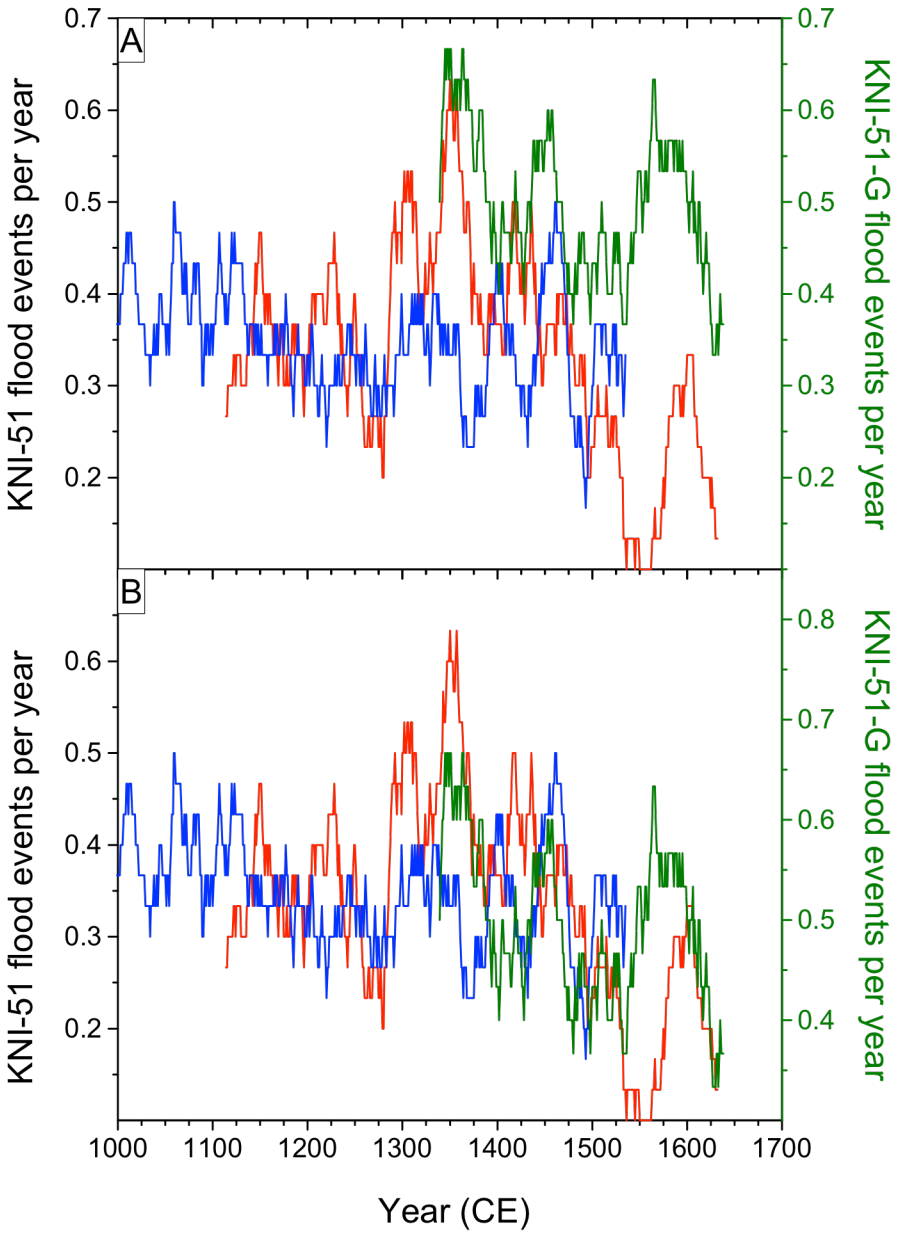

Fig. S12. Comparison of KNI-51-G (right axis) and two coeval stalagmites (left axis) with (A) same scales, and (B) right y-axis compressed to illustrate similar trends between coeval samples. The origin of the elevated numbers of flood layers recorded in stalagmite KNI-51-G is unclear, however the similar trends, both at multi-decadal and multi-centennial scales, suggests that trends in flooding frequency is consistently recorded by each sample.

SI Table 1

Sample	Distance to Base (mm)	^{238}U (ng/g)	^{232}Th (pg/g)	$\delta^{234}U$[a] (corr'd)	Error[b]	$^{230}Th/^{238}U$ (activity)	Error	$^{230}Th/^{232}Th$ (ppm)	Error	Uncorrected Age (yr)	Error (yr)	Corrected Age (yr CE)[c]	Error (yr)
11[d]	405	10,238	1,488	1,338.4	1.1	0.00003	0.00001	3.8	1.5	2	1	2010	1
11	394	5,281	3,046	1,339.0	1.8	0.00009	0.00003	2.5	0.8	4	1	2005	1
11	375	7,458	774	1,341.4	1.6	0.00024	0.00001	38.8	2.0	11	1	1999	1
11	354	5,191	1,382	1,353.5	1.1	0.00058	0.00003	36.3	2.1	27	1	1985	2
11	343	8,557	2,129	1,365.3	1.1	0.00072	0.00001	47.9	1.0	33	1	1979	2
11	334	6,537	2,241	1,366.7	2.4	0.00100	0.00001	48.2	0.9	46	1	1970	2
11	311	6,894	1,505	1,352.4	2.4	0.00138	0.00001	104.6	2.4	64	1	1950	1
11	303	6,311	1,483	1,374.0	2.4	0.00152	0.00002	106.7	2.9	70	1	1945	2
11[d]	297	6,049	643	1,380.3	1.0	0.00139	0.00002	215.5	11.8	64	1	1948	1
11	292	12,297	14,153	1,355.1	0.8	0.00162	0.00001	23.2	0.2	75	1	1949	7
11	280	5,484	137	1,376.3	0.8	0.00165	0.00002	1,091.3	201.8	76	1	1934	1
11	273	11,346	652	1,357.8	2.4	0.00183	0.00001	524.8	22.7	85	1	1928	1
11	266	9,866	513	1,351.3	0.8	0.00177	0.00001	560.6	33.3	82	1	1924	1
11	255	7,711	1,395	1,359.4	1.2	0.00198	0.00001	180.5	3.9	92	1	1921	1
11	231	8,105	2,580	1,345.2	2.3	0.00235	0.00002	122.0	2.3	110	1	1906	2
11[d]	206	6,382	579	1,358.8	1.9	0.00246	0.00003	446.8	32.1	114	1	1896	1
11	200	6,763	2,347	1,360.7	1.0	0.00250	0.00002	119.1	2.4	116	1	1896	2
11[d]	93	4,686	4,432	1,359.9	1.7	0.00472	0.00004	82.4	1.0	219	2	1803	12
11[d]	44	5,321	6,216	1,354.6	1.9	0.00511	0.00005	72.2	0.8	237	2	1787	5
11	24	5,189	7,090	1,323.7	1.4	0.00553	0.00005	66.9	0.7	260	2	1767	17

[a] $\delta^{234}U = [(^{234}U/^{238}U)/(^{234}U/^{238}U)_{eq}-1] \times 10^3$, where $(^{234}U/^{238}U)_{eq}$ is the secular equilibrium activity ratio; values in permil.

[b] Errors at presented at the 2 standard deviation level.

[c] An intial $^{230}Th/^{232}Th$ atomic ratio of $4.4 \times 10^{-6} \pm 50\%$ was used to correct detrital ^{230}Th. Ages also corrected for year of analysis.

[d] These dates previously published in ref. 1 using an initial Th correction of $4.4 \times 10^{-6} \pm 100\%$.